Simulation of irradiation exposure of electronic devices due to heavy ion therapy with Monte Carlo Code MCNP6

Janis Lapins[1], Nicole Guilliard[1,a], Wolfgang Bernnat[2] and Arnulf Buck[3]

[1]*University Stuttgart, Institute for Nuclear Energy and Energy Systems, 70569 Stuttgart, Germany*
[2]*University Stuttgart, KE Technology GmbH, 70569 Stuttgart, Germany*
[3]*Graz University of Technology, Master Student, Austria*

Abstract. During heavy ion irradiation therapy the patient has to be located exactly at the right position to make sure that the Bragg peak occurs in the tumour. The patient has to be moved in the range of millimetres to scan the ill tissue. For that reason a special table was developed which allows exact positioning. The electronic control can be located outside the surgery. But that has some disadvantage for the construction. To keep the system compact it would be much more comfortable to put the electronic control inside the surgery. As a lot of high energetic secondary particles are produced during the therapy causing a high dose in the room it is important to find positions with low dose rates. Therefore, investigations are needed where the electronic devices should be located to obtain a minimum of radiation, help to prevent the failure of sensitive devices. The dose rate was calculated for carbon ions with different initial energy and protons over the entire therapy room with Monte Carlo particle tracking using MCNP6. The types of secondary particles were identified and the dose rate for a thin silicon layer and an electronic mixture material was determined. In addition, the shielding effect of several selected material layers was calculated using MCNP6.

.

1 Introduction

During the last years the treatment of patients with tumours with heavy ions became a big issue. The main advantage compared to the standard treatment with photons is the precise energy deposition in the tissue of the patient [1]. Healthy tissue is barely affected as the heavy ions deposit the majority of their energy at the end of their range in a very sharp Bragg-Peak. The mutated tissue can be scanned step by step to irradiate all tumour regions. But that means that the patient himself has to be immobilized throughout the therapy and a movement of the patient table in the range of millimetres is necessary. BEC Engineering [2] was involved in the development of such a table in the MedAustron Project [3] which allows precise location of the patient with exact minimal movement in any direction. Originally, it was planned to put the electronics for the table outside the room to avoid failure of the electronics due to high irradiation during the therapies. The high dose in the room is a result of secondary particle production. But this is not desirable from a construction point of view. The easiest way of construction would be to keep the electronic control at the table or at least next to it. The question arose how much dose the electronic devices will receive and if this dose rate affects the functions of the systems and which kind of shielding can prevent a high dose deposition in the electronics? The present work focuses on therapies with either carbon ions or protons.

2 Validation of MCNP6 for use with high energy heavy ion simulation

2.1. Validation calculations for carbon ions

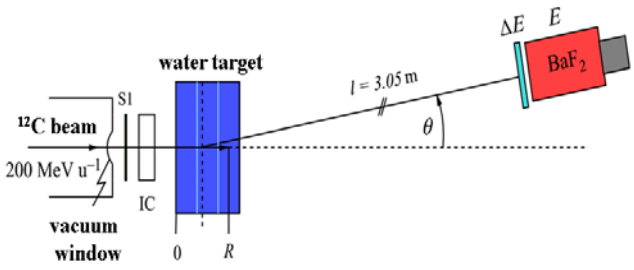

Figure 1: Experimental setup for validation calculations with MCNP6. A carbon ion beam hits a water target producing secondary particles.

[a] Nicole.guilliard@ike.uni-stuttgart.de

To make sure that the production of secondary particles during irradiation is correctly simulated with the selected models implemented in MCNP6 [4] for high energy particles an experiment [5] was recalculated. The experimental setup can be seen in Fig.1. A carbon ion beam with 200 MeV/amu was focused on a water target. The target has a width of about 12 cm. The Bragg peak occurs in the target. The secondary particles were detected in 3.05m behind the Bragg-Peak with a BaF2 detector. The angle between the beam direction and the detector was varied in the range from 0° up to 30°.

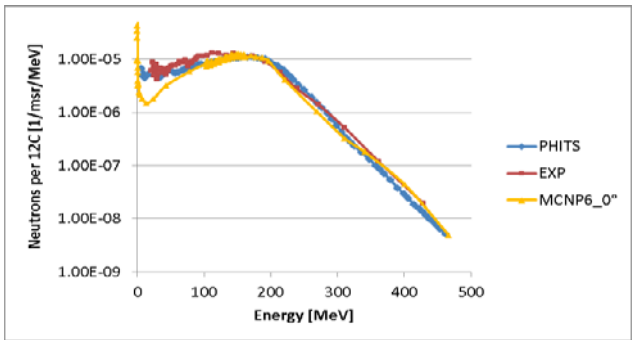

Figure 2: Comparison of the experimental results for secondary neutron production in beam direction (0°) with the simulations in PHITS and MCNP6**.**

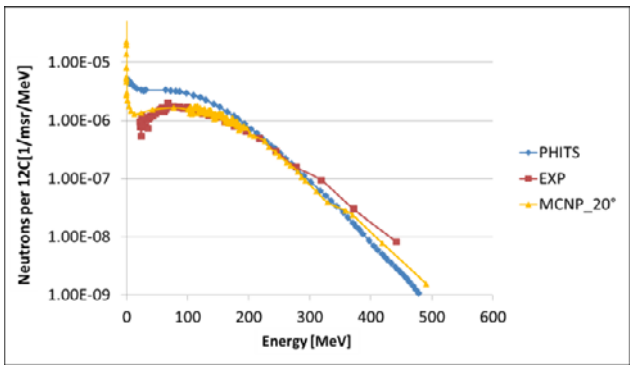

Figure 3: Secondary energy dependent neutron spectrum produced by a C12 ion beam hitting a water target. The experimental results measured at an angle of 20° to the original beam direction are compared with the simulations in PHITS and MCNP6.

In Figure 2 and Figure 3 the experimental results for the production of secondary neutrons are compared to the simulations with the Monte Carlo Code PHITS [5,6] (particle and heavy ion transport code system) and the results obtained with MCNP6 for different angles referred to the incident beam direction. In the high energy region the simulation reproduces the experimental values very accurately. The difference of the detector and the MCNP6 results below 20 MeV are remarkable. The strong rise calculated was not detected. But the detector efficiency in that range is very poor and the experiment does not cover that range properly [7]. The diagrams for other angles show approximately the same behaviour as well as the investigations for other secondary particles like Deuterons, Tritons or Alpha particles (see Figure 4).

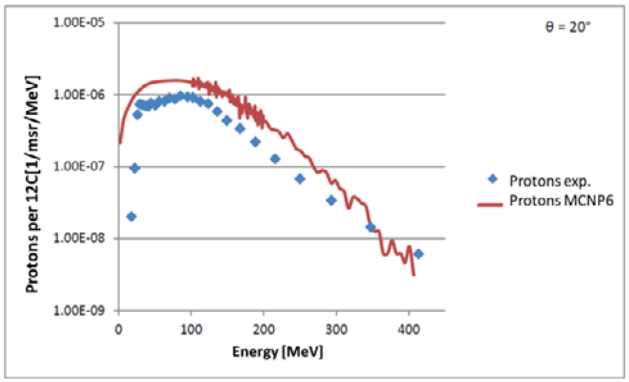

Figure 4: Comparison of experimental and MCNP6 results for secondary proton production in 20° direction**.**

2.1. Validation calculations for protons

Beside therapies with carbon ions it is planned in the MedAustron project to treat patients with protons. To make sure that the used models in MCNP6 provides reliable results for proton source particles and the production of secondary particles additional validation calculations were performed. Due to the leak of open experimental data a code to code benchmark was conducted. The comparative simulation was taken from Agosteo et al. [7]. In this work the secondary particle production for several types of ions on different target materials was investigated. The simulations were performed with the Monte Carlo Code FLUKA [8]. We will compare the results for 215 MeV/u protons impinging a cylindrical ICRU tissue like target [9]. The target length was chosen in such a way that the Bragg peak occurred in the material. The secondary neutrons were detected on a shell surrounding the target and which was divided in 12 angular bins with a width of 15°. Figure 5 shows the results for secondary neutron production as a function of the neutron energy for both the calculation from Agosteo et al [7]. with FLUKA and the ones made at IKE with MCNP6. The results for four different angle bins are plotted (0°-15°, 30°-45°, 60°-75°, 165°-180°, relative to the incident beam). The spectra in the different directions do not differ significantly and show more or less the same behaviour. A slight decrease of neutron production can be observed in the high energy region with increasing angles to the beam direction with both codes, especially for backscattered particles with an angle larger than 165°. In this energy region the results of the simulations do not agree as well as in the very low energy region. As both tools are Monte Carlo Codes and as the total amount of back scattered particles is much lower than the amount of particles in forward direction the statistical error increases with larger angles. The large fluctuations in the thermal energy region indicate that the results have large statistical errors as the amount is very low. But all together the code to code benchmark validates that the used MCNP6 models are an appropriate tool for the analysis of secondary particle production in proton therapy.

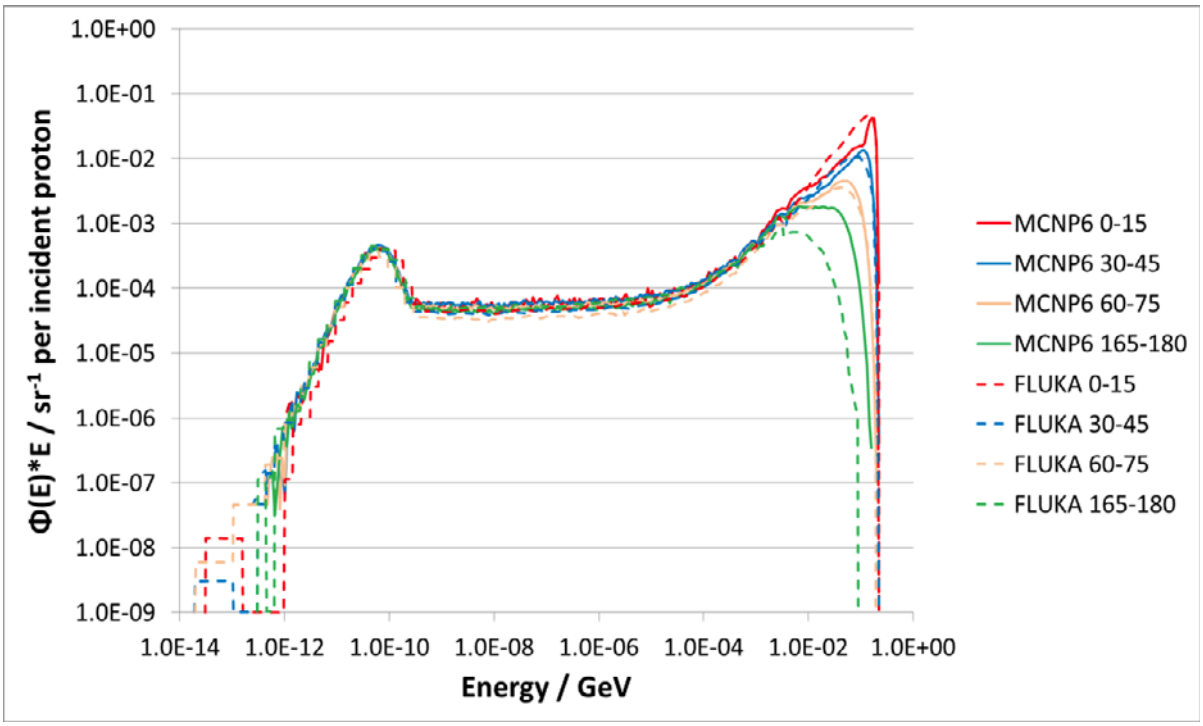

Figure 5: Spectrum of secondary neutrons for certain angles after irradiation of a tissue target with 215 MeV/u protons.

3 Response functions

The MCNP6 simulation for heavy ion irradiations with production of secondary particles tracks the particle way through the geometry and gives an energy dependent flux value Φ for every point of the geometry and for each particle type. To estimate a dose D which is deposited in a certain material the user needs to define response functions *f(E)* for all interesting particle types. With the simulated flux for different particles *i* the total deposition in this material can be calculated for every location in the room.

$$D_x = \sum_{i=1}^{n} \phi_i(E) f_{x,i}(E) dE \qquad (1)$$

The deposited energy depends also on the material thickness *x* as particles like protons and alphas have sharp Bragg-Peaks and release the majority of their energy at a certain depth or high energy particles can cross thin layers without any interaction. To determine the response function for a certain particle type, simulations with an isotropic point source and a distinct energy of the source particles are performed for the energy region of interest. By varying the source energy an energy dependent response function can be generated. To obtain a complete set of response functions the calculations were made for several particle types such as neutrons (n), protons (h), deuterons (d), tritons (t), electrons (e) photons (p), He-3 (s) and He-4 (a).

Fig. 6 shows the response function for neutrons (n) for Silicon layers with different thicknesses s. The function is normalized to one gram of silicon. The response function depends on the target thickness. As the way through a thick target is longer, the reaction possibility is higher. Same applies to the secondary particles that travel a longer distance inside the sample. Even though very high energetic neutrons can pass the target without any interaction the response function increases in the high energy region. This is due to the fact that the deposition per interaction rises. So although the number of events decreases the energy transfer of a single event deposits an enormous amount of energy. The peak in the thermal energy region arises from non-elastic reactions. In the high energy region the energy transfer is dominated by elastic scattering and spallation reactions.

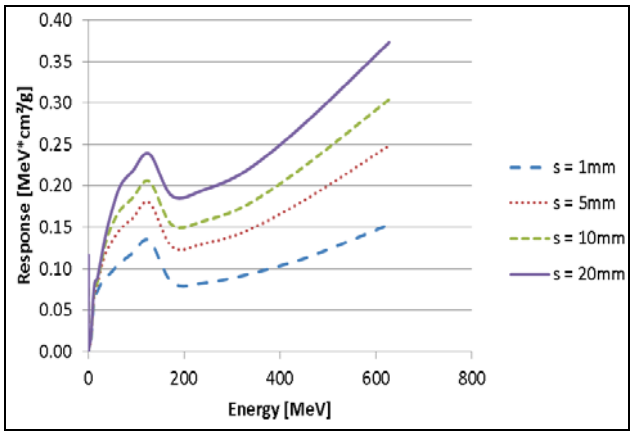

Figure 6: Response function of neutrons for Si layers with different thickness.

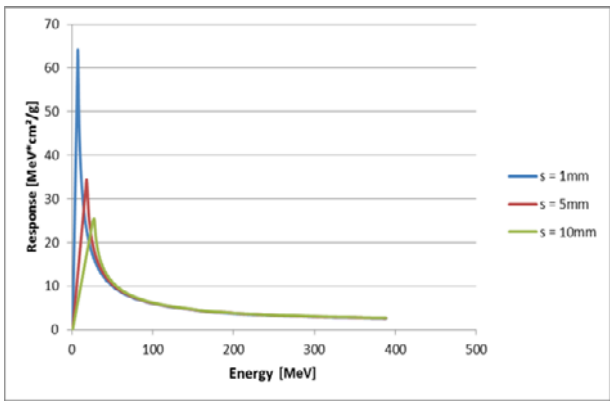

Figure 7: Response function of protons for Si layers with different thickness.

Figure 7 shows the response functions for protons (p) hitting Silicon layers of different thicknesses. Compared to the results for neutrons, the response of protons differs by a power of ten although the particles have comparable masses. Generally, the interaction possibility is strongly affected by the charge of the particles. For heavy particles (compared to the electron mass) the energy transfer can be described by the Bethe-Bloch formula. The formula says that the energy transfer $-dE/dx$ is proportional to the square of the charge z and reciprocal proportional to the square of the particle velocity v:

$$-\frac{\mathrm{dE}}{\mathrm{dx}} \propto \frac{z^2}{v^2} \qquad (2)$$

Figure 7 also shows that the maximum of the response tends to higher energies for thicker targets. Above a certain energy the Bragg peak occurs beyond the length of the thin layer and the particles pass the target without strong interactions. The decreasing maximal value can be explained by the fact that the values are normalized to one gram of Silicon. In fact, the total energy release in a thick layer is higher than in a thin layer. In the energy region where all neutrons pass even the thick layer without interaction the curves coincide as the energy transfer is constant along the way and therefore proportional to the mass.

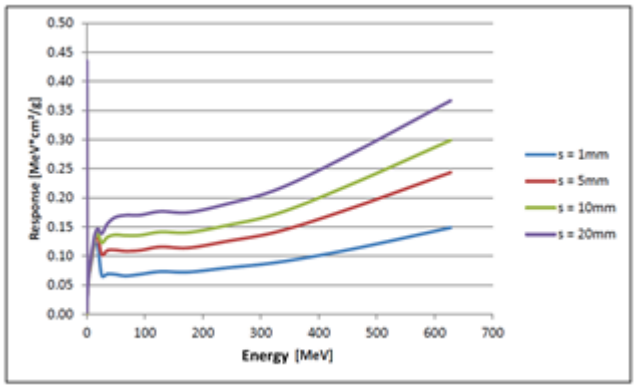

Figure 8: Response function of neutrons for electrical device with different thickness.

The functions were also determined for a material mix consisting of typical materials used for electronic devices (see figure 8). But only small differences were identified. The higher response in the thermal energy region can be explained by the larger capture cross sections of iron and copper. For high energies the response function is very similar to the one calculated for Silicon Hence, the following simulations and results apply to depositions in Silicon.

4 Simulations of radiation exposure to the electrical devices in a therapy room with MCNP6

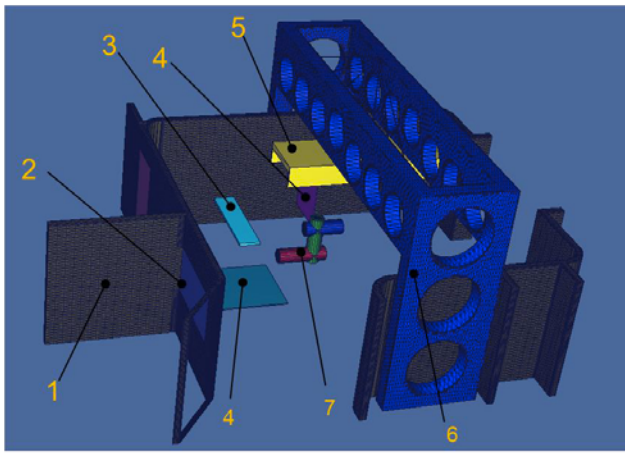

Figure 9: 3-D model of the room for MCNP6 without floor, ceiling and concrete walls. 1) wooden wall, 2) Lead window, 3) table, 4) Si plate for deposition, 5) linear axle, 6) supporting structure, 7) robot arm.

A typical therapy room was modelled with MCNP6 Figure 9 shows the interior of the room without the surrounding concrete wall, the floor and the ceiling. The most important components are modelled as simple geometric bodies. Next to the patient table (no.3) is the robot arm (no.7) for positioning which is connected to the linear axle (no.5) and the supporting structures (no.6). For deposition simulations a patient model is taken from former investigations of the Argonne National Laboratory (ANL) [11] consisting of a simplified body with typical human tissue and skeleton material.

Figure 10 is a cross section of the room at the level of the patient during therapy sessions. The red arrow shows the beam direction of the heavy ions in case of Carbon therapy. The orange dot next to the patient represents the robot arm. The thin blue lines are the wooden partition panels. The cross section also shows the thick concrete walls surrounding the room in light blue. During the carbon ion therapy the beam comes from the left side (figure 9) whereas in case of proton therapy the beam can be adjusted for irradiation from top to bottom. Below the table is a cavity in the floor where a camera for positioning of the patient should be located.

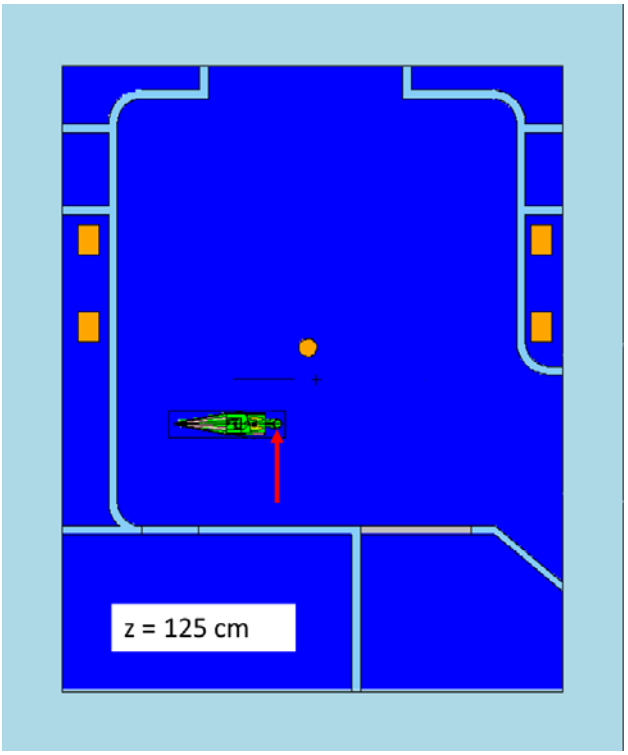

Figure 10. Cross section of the simulated therapy room in MCNP6 at a height of 125cm.

To estimate the deposition during the irradiations with a cell tally a plate of Silicon is simulated below the table. Additional Si-cells for cell tally measurements were located next to the robot arm (between position 4 and 7) and above the linear axle (position 5) as those places are preferred positions for electrical devices. The results of the cell tally measurements can be compared to those obtained by a flux mesh tally covering the whole room using the response functions. The simulations were performed using the response functions for a 0.1 mm thick Si layer. Considered particles are those mentioned above: neutrons, electrons, photons, deuterons, tritons, helions, alphas and heavy ions. To normalize the deposited dose during one year of operation some assumption were made. These are summarized in table 1.

Table 1. Assumptions for normalization of the cumulated dose after one year of irradiation.

	Carbon ions	**Protons**
Number of patients per year	800	800
Intensity	$4*10^8$ Ions/pulse	$4*10^{10}$ Ions/pulse
Pulse frequency	0.5 Hz	0.5 Hz
Duration of one irradiation	45 min	45 min
Starting particles per year	$4.32*10^{14}$	$4.32*10^{16}$

Carbon ions with 200 MeV/u

Figure 11 gives an overview of the deposited dose for irradiation with 200MeV/amu carbon ions after one year in the layer containing the initial ion beam. The highest dose occurs in beam direction, as expected. The robot arm shields part of the secondary particles and a lower dose is expected behind the apparatus. Another decrease of dose can be seen behind the human body on the left side of Figure 10 due to the absorption of secondary particles in the patient.

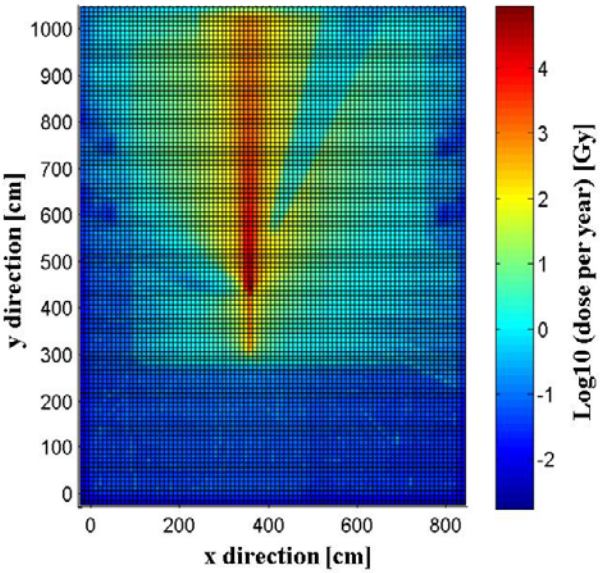

Figure 11. MCNP6 calculation of the dose deposited in a 0.1 cm thick Si layer after one year Carbon ion therapy with 200 MeV/u.

The cross section of the mesh tally in yz-direction is shown in figure 12. The dose per year upon the linear axle and on the left side of the room (beam entry) is more than a factor of 10^4 smaller than the dose expected in beam direction. The heavy particles are mainly scattered in forward direction. Therefor the installation of sensitve electrical devices on top of the axle is more advisable than put it directly next to the robot arm. Assuming a limit of 10^2 Gy/year it is recommended to avoid the red and orange locations for very sensitve devices.The wooden panel at y=300cm shields the backscattered particles and leads to a very small dose rate in the anterroom. To know which particle type is mostly responsible for the deposition the percental fraction of the different types was identified. It was found that the deposition in forward direction near the patient originates predominantely from heavy ions, alphas and protons (figure 13). The deposition caused by photons, electrons and neutrons can be neglected.

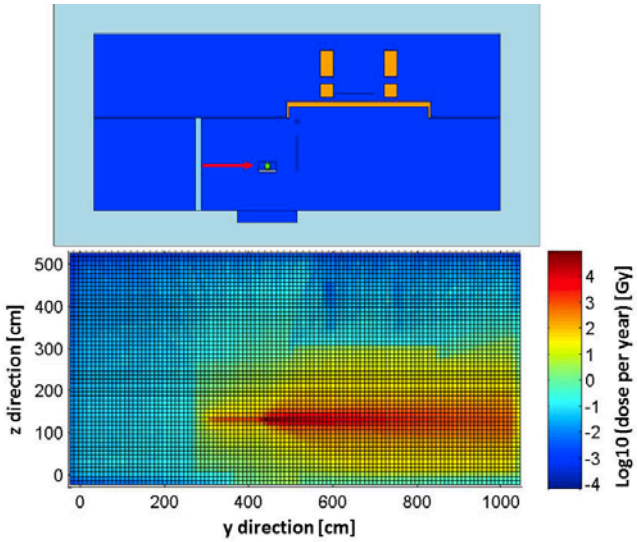

Figure 12. *top*: yz-cross section of the therapy room. *bottom*: MCNP6 calculation of the dose deposited in a 0.1 cm thick Si layer after one year Carbon ion therapy with 200 MeV/u.

In the upper and lower part of the room with an increasing angle to the original beam the influence of the heavy particles gets lower and most of the deposition comes from protons, electrons and photons (figure 14). The results of the MCNP6 cell detectors were used for comparison and validation of the mesh tally method and showed good agreement with the mesh tally results. The deposited energy during one year above the linear axle calculated with the cell tally was $2.17*10^{-1}$ Gy and the dose for one year at the position next to the robot arm was about $1.88*10^{3}$Gy. This confirms the results obtained by the mesh tally in figure 11 and figure 12.

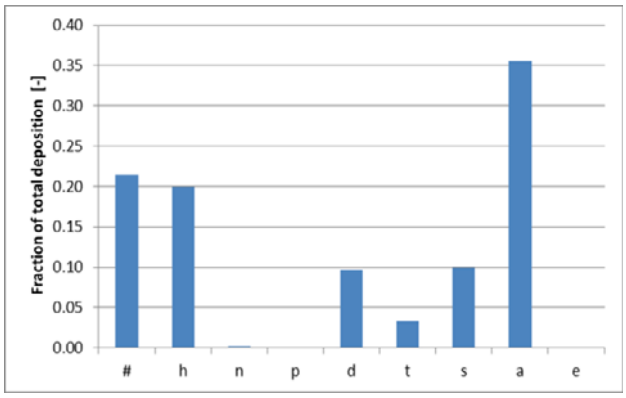

Figure 13. Fraction to the total deposition in a Si-layer of different particle types during a heavy ion therapy with C12 ions at the robot arm. (#: heavy ions, h: protons, n: neutrons, p: photons, d: deuterons, t: tritons, s: He-3, a: He-4, e: electrons).

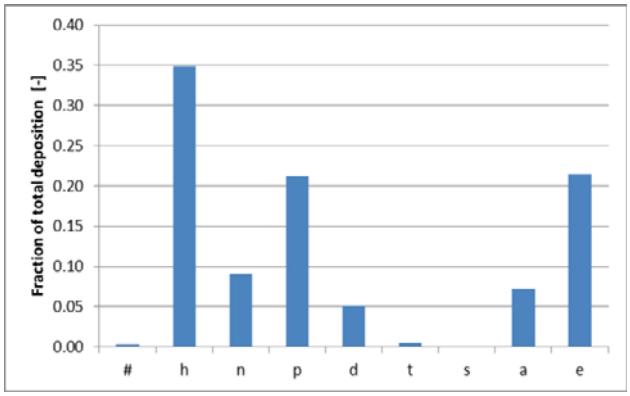

Figure 14. Fraction to the total deposition in a Si-layer of different particle types during a heavy ion therapy with C12 ions above the linear axle.

Protons with 250 MeV/u

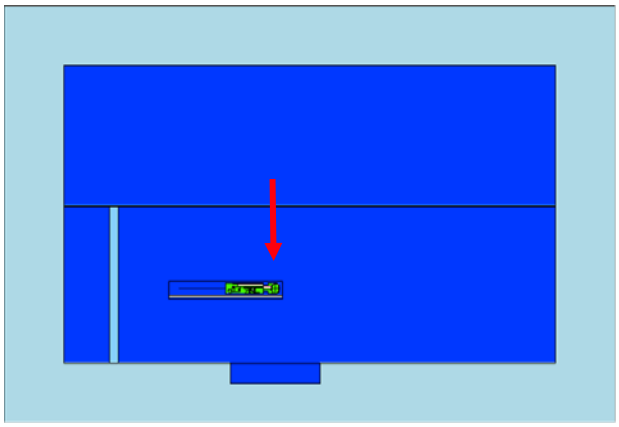

Figure 15. Axial cut of the therapy room in the beam plane simulated with MCNP6.

Analogue calculations were made for irradiation therapy with 250MeV protons. The assumptions for normalization of the accumulated dose after one year of therapy can be found in table 1. The geometry modeling of the room and the patient are the same as the one used for the former calculation with carbon ions. The proton beam direction is changed and goes from top to bottom (see figure 15) as forseen in the planning of the irradiation centre. The energy of the protons is 250Mev/amu. figure 15 shows the cumulated dose after one year of proton therapy deposited in a 0.1mm thick Silicon layer. The absolute deposited energy is about 100 times higher than for carbon ions due to the higher intensity of the protons during irradiation (see table 1). Again the region above the linear axle seems to be most favourable as location for electrical devices. The asymmetric distribution at z=125cm on the left side of the beam shows the position of the phantom. Below the table a cavity can be seen. The camera necessary for the exact positioning of the patient should be placed at this

location. To check the results, standard track tallies were used that are implented in MCNP6. The flux in a cell volume is estimated by track length. Results with cell detector in the cavity was 2.72*10^{3}Gy. This value seems to be very low compared to the meshtally results in figure 16. But the cell tally covers the whole cavity. The average dose of the mesh tally calculation over the whole cavity is in acceptable agreement (as can be seen in figure 17). Although the dose rate in the cavity is very high the camera has to be placed there for technical reasons. But it might help to avoid the position in direct beam direction. A slight shift may helb to decrease the deposition.

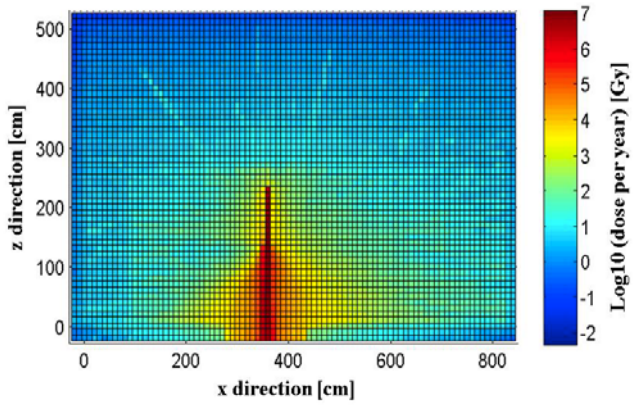

Figure 16. MCNP6 calculated deposition in a 0.1cm thick Si layer after one year therapy with 250MeV protons.

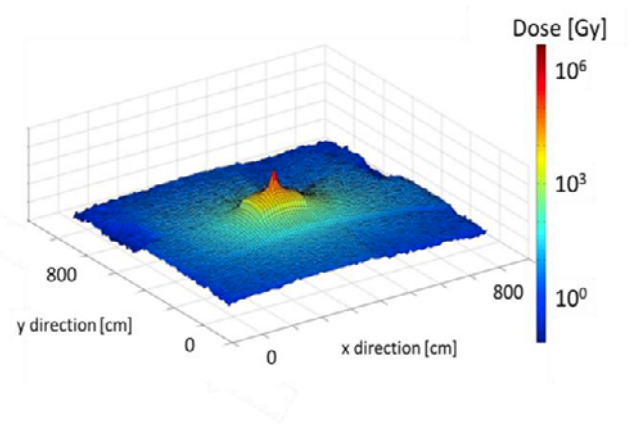

Figure 17. MCNP6 calculated deposition in a 0.1cm thick Si layer after one year therapy with 250MeV protons. The region around the cavity under the table is shown at z level of the cavity.

5 Shielding

To investigate which shielding materials can protect the electronic devices simulations with a simplified model were performed. A tissue like target is pounded with ^{12}C ions with an energy of 200 MeV/u and protons with an energy of 250 MeV/u. The dose deposited in a one cm thick Silicon layer behind a shielding layer was compared to the dose deposited without any shielding. The tissue target has a thickness of about 18cm (see figure 18). A set of different materials were determined. Beside the typical neutron absorbers like boron (B) and Gadolinium (Gd), polyethylene (PE) as well as heavy materials like concrete, lead (Pb) and iron (Fe) were used. Figure 19 gives a summary of the results in the case of carbon source particles. As figure 13 already indicated, most of the deposition is caused by heavy charged particles. Therefore, the best shielding effect is obtained with heavy elements, whreas the light shielding materials like boron granulate (boron mixed with carbon) or Polyethlene reduced the original dose without shielding only by a factor of 2/3.

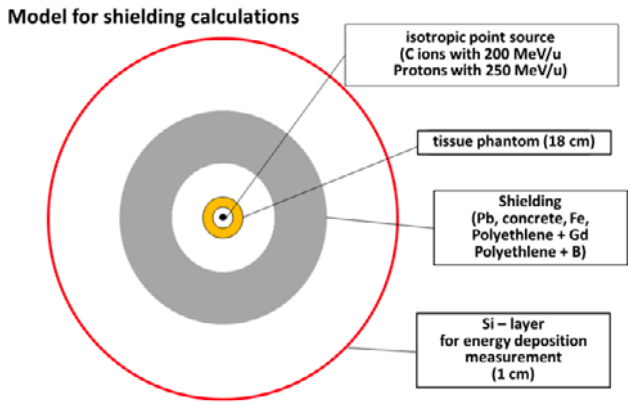

Figure 18. Setup for the simulation of a C12 ion beam impinging a tissue target. Different particle types are measured in a Si layer with and without shielding.

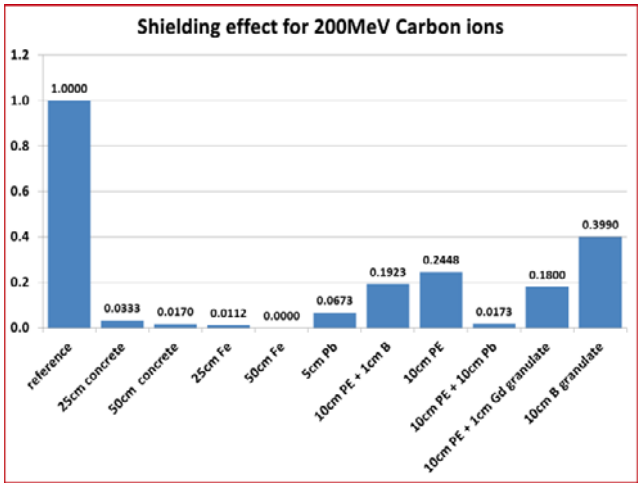

Figure 19. Comparison of the shielding effect of selected materials for the secondary particles produced by carbon ions with 200 MeV/u impinging a tissue target.

The same model and shielding materials were used for 250 MeV/u protons as source particles. Again the thick heavy shielding materials provides the best shielding effect (see figure 20). An interesting behaviour can be

observed using exclusively light materials. The relative dose after the shielding is increased. It seems as there are a lot of new secondary particles produced when the protons pass the Silicon layer.

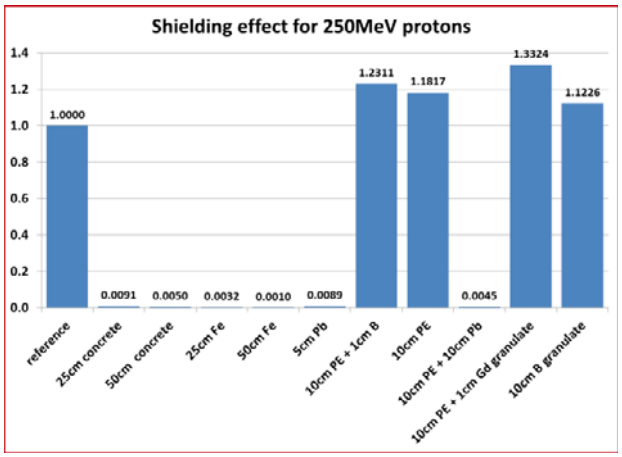

Figure 20. Comparison of the shielding effect of selected materials for the secondary particles produced by protons with 250 MeV/u impinging a tissue target.

6 Conclusion

It was shown that MCNP6 is an adequate tool for estimating the production of secondary particles and to estimate the energy deposition in strucutres during heavy ion therapy. The dose rate in beam direction is very high and it is questionable to put sensitve electrical devices there. Increasing the angle between the beam direction and the point of intrest can help to reduce the dose significantly. Additional shielding installation can protect sensitive electrical devices. The best shielding effect is achieved by heavy thick material which comes along with unhandy constructions. Therefore it would be much easier to use light material. But for light material shieldings it is important to know the exact position and particle type to get an optimized shileding. The impact on dose reduction may be sufficient for Carbon ions but can be a bad choice in case of proton therapy.

Acknowledgment

We thank the colleauges from Buck Engineering & Consulting GmbH who initiates this interesting collaboration and provided technical data for the calculations.

References

1. G. Kraft, “Tumor therapy with heavy charged particles”, Prog. Part. Nucl. Phys. **45**, p473-544,(2000).
2. Buck Engineering & Consulting GmbH, 72764 Reutlingen (Germany)
3. E. Griesmayer, T. Schreiner und M. Pavlovic, „The MedAustron project,“ Nucl. Instr. and Meth. in Phys. Res. **B 258**, pp. 134-183, (2007).
4. D.B. Pelowitz (Ed.), “MCNP6^{TM} User’s Manual Version 1.0,” LA-CP-13-00634, Rev. 0 (2013).
5. K. Gunzert-Marx, H. Iwase, D. Schardt, R. S. Simon, „Secondary beam fragments produced by 200 MeV/u ^{12}C ions in water and their dose contributions in carbon ion radiotherapy,“ New Jour. of Phys. (2008) 075003 (21pp).
6. H. Iwase, K. Niita, T. Nakamura: "Development of general-purpose particle and heavy ion transport Monte Carlo code", J. Nucl. Sci. and Technol. 39, 1142 (2002).
7. S. Agosteo, A. Mereghetti, E. Sagia, M. Silari, “Shielding data for hadron-therapy ion accelerators: Attenuation of secondary radiation in concrete”, Nucl. Instr. and Meth. in Phys. Res. **B 319**, pp. 154-167 (2014).
8. A. Ferrari, P.R. Sala, A. Fassò, J. Ranft, FLUKA: a multi-particle transport code, CERN-2005-10, 2005, INFN/TC_05/11, SLAC-R-773.
9. International Commission on Radiation Units and Measurements, Report No. **33**, Bethesda, Maryland, USA, 1980 p. 20.
10. K. Gunzert-Marx, “Nachweis leichter Fragmente aus Schwerionenreaktionen mit einem BaF2-Teleskop-Detektor”, Diss. D17, TU Darmstadt (2004)
11. D. Krstic und D. Nikezic, „Input files with ORNL-mathematical phantoms of the human body for MCNP-4B“,Computer Physics communications **176**, pp. 33-37 (2007).